Postsynaptic TrkB signaling has distinct roles in spine maintenance in adult visual cortex and hippocampus

Sridhara Chakravarthy*, M. Hadi Saiepour*, Matthew Bence*, Sean Perry*†, Robin Hartman*, Jonathan J. Couey‡, Huibert D. Mansvelder‡, and Christiaan N. Levelt*§

*Department of Molecular Visual Plasticity, Netherlands Ophthalmic Research Institute, Royal Netherlands Academy of Arts and Sciences, Meibergdreef 47, 1105 BA, Amsterdam, The Netherlands; and ‡Department of Experimental Neurophysiology, Center for Neurogenomics and Cognitive Research (CNCR), Vrije Universiteit, De Boelelaan 1085, 1081 HV, Amsterdam, The Netherlands

Edited by William T. Greenough, University of Illinois at Urbana–Champaign, Urbana, IL, and approved November 30, 2005 (received for review July 24, 2005)

In adult primary visual cortex (V1), dendritic spines are more persistent than during development. Brain-derived neurotrophic factor (BDNF) increases synaptic strength, and its levels rise during cortical development. We therefore asked whether postsynaptic BDNF signaling through its receptor TrkB regulates spine persistence in adult V1. This question has been difficult to address because most methods used to alter TrkB signaling *in vivo* affect cortical development or cannot distinguish between pre- and postsynaptic mechanisms. We circumvented these problems by employing transgenic mice expressing a dominant negative TrkB–EGFP fusion protein in sparse pyramidal neurons of the adult neocortex and hippocampus, producing a Golgi-staining-like pattern. In adult V1, expression of dominant negative TrkB-EGFP resulted in reduced mushroom spine maintenance and synaptic efficacy, accompanied by an increase in long and thin spines and filopodia. In contrast, mushroom spine maintenance was unaffected in CA1, indicating that TrkB plays fundamentally different roles in structural plasticity in these brain areas.

adult cortical plasticity | BDNF signaling | synapse stability | transgenic mice

During development, synapse formation and elimination are regulated by molecular cues, spontaneous activity, and experience (1, 2). Most glutamatergic synapses on excitatory neurons are situated on dendritic spines. Live imaging of neurons expressing GFP has provided important information on the dynamics of spine formation and maintenance (3–8). Filopodia are short-lived finger-shaped protrusions and believed to be precursors of dendritic spines (9, 10). Newly formed spines are often thin or long and appear and disappear within days. Some mature into mushroom or stubby spines, which are more stable and often persist for months (7, 8). There are strong correlations between spine size, spine persistence, synaptic efficacy, and the number of α-amino-3-hydroxy-5-methyl-4-isoxazolepropionate receptors (AMPARs) at the postsynaptic density (8, 11, 12). With development and aging of the cortex, there is a shift toward larger and more persistent spine types (3, 7, 13).

Spine dynamics are influenced by plasticity. Long-term potentiation in hippocampus is associated with an increase in spine size (14) and spine formation (15), whereas term depression is associated with spine elimination (16). Interestingly, reducing synaptic input results in an increase in spine numbers, probably due to homeostatic mechanisms (17–19).

Ocular dominance plasticity in V1 is associated with initial pruning and later formation and stabilization of spines (20, 21) and occurs predominantly during a critical period of development. Maturation of the extracellular matrix is a major factor in ending the critical period, probably by increasing spine and axon stability (20–22)

BDNF signaling through TrkB receptors is a key player in visual plasticity (23, 24). It drives the development of inhibitory innervation, an important factor in ocular dominance plasticity (25, 26). BDNF is also implicated in directly effecting structural (27–29) and functional changes (30–34) in excitatory neurons. Several studies indicate that postsynaptic TrkB signaling stimulates the formation and maturation of spines (35, 36). As BDNF expression rises in V1 upon eye opening and reaches maximal levels at early adulthood (26, 37), increased TrkB-signaling may determine the increased spine persistence observed in adult V1. However, a recent study indicated that, whereas postsynaptic TrkB signaling is essential for synapse formation in developing hippocampal neurons, it is dispensable for spine maintenance in adult CA1 (38). Whether the same holds true for adult V1 is currently unknown.

To resolve this issue, we set out to analyze the roles of postsynaptic TrkB signaling in spine maintenance in adult V1 and CA1. This problem has been difficult to address because the various methods used for altering TrkB signaling *in vivo* also affect cortical development or do not allow dissection of pre- and postsynaptic mechanisms. We bypassed these problems by employing transgenic mice expressing an EGFP fusion protein of the truncated TrkB receptor (TrkB.T1–EGFP), which acts as a dominant negative receptor (39) or a membrane-associated EGFP (EGFP-F) in sparse pyramidal neurons in the adult neocortex and hippocampus starting 6 weeks after birth. This Golgi-staining-like expression pattern permitted us to study structural modifications in pyramidal neurons mediated by postsynaptic inhibition of TrkB signaling, without disrupting development of the cortical circuitry or extracellular matrix. We provide evidence that postsynaptic TrkB signaling is a key determinant of spine maintenance in adult V1 but has much less influence on spines in CA1.

Results

Expression of EGFP-F or TrkB.T1–EGFP in Individual Neurons of the Adult Brain. To express EGFP-F or TrkB.T1–EGFP in comparable, individual pyramidal neurons in the adult cortex and hippocampus, three transgenic mouse lines were created. The first line, Cre-3487, carried a Cre transgene under the control of the calcium/calmodulin-dependent kinase IIα (CaMKIIα) promoter and defined the Golgi-staining-like expression pattern. The other lines, TLG 498 and TLT 817, defined what protein was expressed in a Cre-dependent fashion, i.e., EGFP-F or TrkB.T1–EGFP respectively. In mice double transgenic for CaMKIIα-Cre and TrkB.T1–EGFP or EGFP-F, EGFP fluorescence was detected in isolated pyramidal neurons in layers II/III and V of the neocortex and pyramidal and granule cells of the hippocampus, starting around 6 weeks after birth and accumulating during the following weeks (Fig. 1 *A* and *B*).

Conflict of interest statement: No conflicts declared.

This paper was submitted directly (Track II) to the PNAS office.

Abbreviations: AMPAR, α-amino-3-hydroxy-5-methyl-4-isoxazolepropionate receptor; EGFP-F, membrane-associated EGFP; CaMKIIα, calcium/calmodulin-dependent kinase IIα; mEPSC, miniature excitatory postsynaptic current; LSL, lox-Stop-lox.

†Present address: Picower Center for Learning and Memory, Massachusetts Institute of Technology, 77 Massachusetts Avenue, Cambridge, MA 02139-4307.

§To whom correspondence should be addressed. E-mail: c.levelt@ioi.knaw.nl.

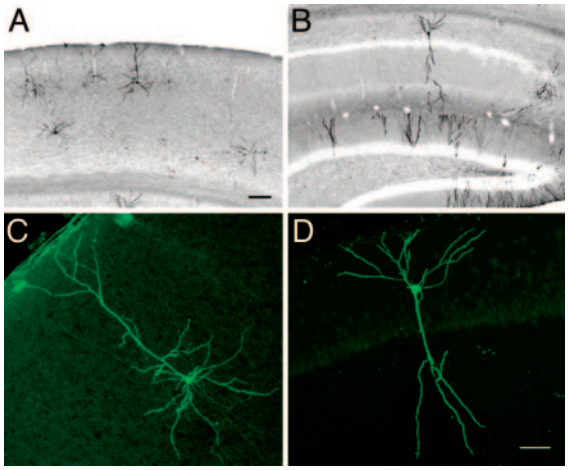

Fig. 1. Expression of TrkB.T1–EGFP in adult visual cortex and hippocampus. (*A*) TrkB.T1–EGFP expression in primary visual cortex (V1) is mosaic and restricted to pyramidal neurons of layer II/III and V. (*B*) In hippocampus, TrkB.T1–EGFP expression occurs in pyramidal cells and granule cells. Inverted grayscale images of Cy3-fluorescence are shown. A higher magnification of TrkB.T1–EGFP pyramidal neurons in V1 (*C*) and CA1 (*D*) show expression in all cellular compartments. [Scale bars: 100 μm (*A–B*) and 50 μm (*C–D*).]

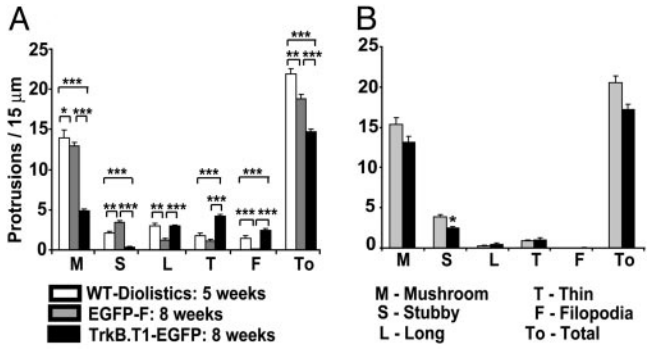

Fig. 3. TrkB.T1–EGFP-expressing neurons in V1, but not in CA1, have less mushroom and stubby spines and more filopodia. (*A*) V1 total protrusions. TrkB.T1–EGFP-expressing pyramidal cells in V1 show a 60–85% reduction in mushroom and stubby spines, a 2- to 3-fold increase in thin and long spines, and a 22-fold increase in filopodia. In comparison with 5-week-old WT neurons labeled with DiI, TrkB.T1–EGFP-expressing neurons have 65% fewer mushroom and stubby spines and more thin spines (2.3×) and filopodia (1.7×). (*B*) CA1 total protrusions. In CA1 pyramidal cells, stubby spines are reduced by 35%. No significant differences were found in other protrusions. Error bars represent SEM. ***, ($P < 0.0001$); **, ($P < 0.005$); *, ($P < 0.05$). n = 3,417 spines for V1; 989 spines for CA1; and 328 spines for 5-week-old V1.

Comparable expression patterns were observed in mice double transgenic for CaMKIIα-Cre and TrkB.T1–EGFP or EGFP-F although recombination was less efficient in TrkB.T1–EGFP mice. Representative sections of TrkB.T1–EGFP-expressing neurons in V1 and CA1 are shown in Fig. 1 *C* and *D*. To ensure that the observed mosaicism was mediated by Cre-3487 and was not inherent to the EGFP-F or TrkB.T1–EGFP transgenes, we confirmed that, when crossed to broad Cre-expressing lines, TLG 498 and TLT 817 showed transgene expression in most pyramidal neurons (data not shown).

Both TrkB.T1–EGFP and EGFP-F were detected in all compartments of the cell, including the spines (Fig. 2 *A–D*) and axons. Biocytin injections showed that all dendritic protrusions were labeled with EGFP-F (Fig. 2 *E–G*) or TrkB.T1–EGFP (Fig. 2 *H–J*). This observation excludes the possibility that spines of EGFP-F- or TrkB.T1–EGFP-expressing neurons appeared different due to variation in EGFP localization. Altogether, these transgenic mice were well suited for studying the different spine types in adult V1 and CA1 neurons.

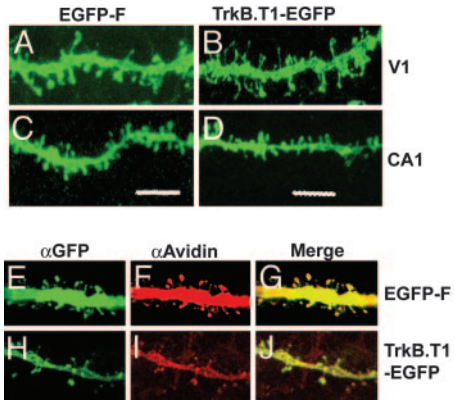

Fig. 2. EGFP-F and TrkB.T1–EGFP label all dendritic protrusions. High magnification projections of confocal images of dendritic protrusions from V1 neurons expressing EGFP-F (*A*) and TrkB.T1–EGFP (*B*) show that distinct protrusions are labeled. Similar labeling was observed in EGFP-F-expressing (*C*) and TrkB.T1–EGFP-expressing (*D*) neurons of CA1. Confocal sections of biocytin-filled EGFP-F-expressing neurons stained for αGFP (*E*) and αAvidin-Cy3 (*F*) show that all protrusions are labeled with both GFP and biocytin (*G*). Comparable images for TrkB.T1–EGFP are represented (*H–J*). (Scale bar: 5 μm.)

TrkB.T1–EGFP Expression Reduces Mushroom Spines and Increases Long and Thin Spines and Filopodia in V1 but Not in CA1. To test whether expression of TrkB.T1–EGFP had any effects on spine morphology in adult V1, pyramidal neurons in layer II/III of 8-week-old transgenic mice were analyzed by confocal microscopy. At this age, the cells had expressed the transgene for up to 2 weeks. Dendritic protrusions on basal and proximal and distal apical dendrites were classified in different spine categories (mushroom, long, thin, or stubby) or as filopodia and counted (see Fig. 7*B*). Compared with EGFP-F-expressing neurons, mushroom and stubby spines of TrkB.T1–EGFP neurons were reduced by 60% and 85%, respectively ($P < 0.0001$; Fig. 3*A*). On the other hand, there were 2–3 times more long and thin spines ($P < 0.0001$) and 22 times more filopodia ($P < 0.0001$). The total density of protrusions was reduced by 24% ($P < 0.0001$). Protrusion changes in apical and basal dendritic segments were similar (data not shown).

These results suggested that, from the onset of TrkB.T1–EGFP expression, the density of mushroom and stubby spines declined, whereas thin and long spines and filopodia increased. To verify this finding, we assessed the densities of different spine types before the onset of TrkB.T1–EGFP expression (6 weeks of age). Neurons in V1 from 5-week-old WT mice were labeled with DiI by using diolistics. At this age, the critical period is just closing and spine morphologies are becoming similar to the adult situation. We detected a slightly higher density of mushroom spines than in adult EGFP-F-expressing neurons (7.8%, $P < 0.05$, Fig. 3*A*). In addition, we detected higher densities of long spines (2.4-fold, $P < 0.005$) and filopodia (20-fold, $P < 0.0001$) but a 40% lower density of stubby spines ($P < 0.005$) than in adult EGFP-F-expressing neurons. In most respects TrkB.T1–EGFP-expressing neurons in adult V1 resembled pyramidal neurons in 5-week-old V1 more than those in adult V1. However, even compared with neurons in younger V1, TrkB.T1–EGFP-expressing cells showed a 65% reduction of mushroom and stubby spines ($P < 0.0001$) and an increase in thin spines (2.3-fold, $P < 0.0001$) and filopodia (1.7-fold, $P < 0.0001$). The fact that the density of long spines on TrkB.T1–EGFP-expressing neurons was similar to their density in pyramidal neurons in 5-week-old V1 may indicate that reduced TrkB signaling inhibits

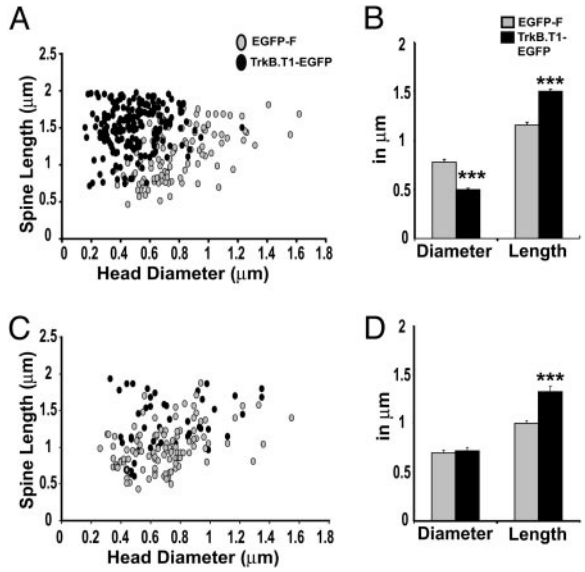

Fig. 4. TrkB.T1–EGFP expression influences spine length and head size in V1. (*A*) Correlation plot of spine head diameter and spine length shows that, in V1, TrkB.T1–EGFP expression results in the loss of the largest mushroom spines and a shift toward longer spines with smaller heads. (*B*) The mean head diameter of mushroom spines on TrkB.T1–EGFP-expressing neurons in V1 is reduced by 40% whereas their length is increased by 30%. (*C*) In CA1, TrkB.T1–EGFP expression does not affect spine head size but does result in increased numbers of spine length among spines with small heads. (*D*) In CA1, mushroom spines of TrkB.T1–EGFP-expressing neurons do not show a difference in the mean spine head diameter but are 32% longer. Error bars represent SEM. ***, $P < 0.0001$.

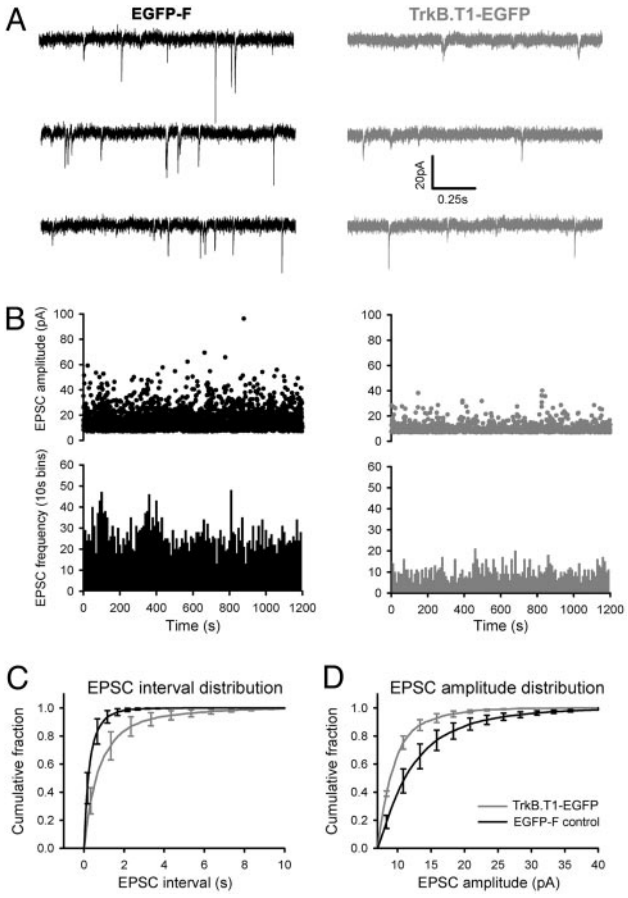

Fig. 5. Reduced mEPSC amplitude and frequency in V1 neurons of TrkB.T1–EGFP. (*A*) Two sets of typical recordings from EGFP-F and TrkB.T1–EGFP-expressing neurons. (*B*) Distribution of mEPSC amplitudes in two typical recordings in EGFP-F-expressing (*Upper Left*) and TrkB.T1–EGFP-expressing (*Upper Right*) neurons and their corresponding mEPSC frequencies (*Lower*). (*C*) Cumulative probability distribution of inter-event (mEPSC) interval in EGFP-F and TrkB.T1–EGFP-expressing neurons. The frequency in TrkB.T1–EGFP-expressing neurons was significantly reduced ($P < 0.0001$, KS-Z = 11.28). Median interval was 0.19 ± 0.09 s in EGFP-F and 0.62 ± 0.11 s in TrkB.T1–EGFP-expressing neurons. (*D*) Cumulative probability distribution of mEPSC amplitude in EGFP-F and TrkB.T1–EGFP-expressing neurons. The amplitude was significantly reduced in TrkB.T1–EGFP-positive neurons ($P < 0.0001$, KS-Z = 7.44). Median amplitude was 10.95 ± 0.07 pA and 8.9 ± 0.3 pA in EGFP-F and TrkB.T1–EGFP positive neurons, respectively. Error bars represent SEM.

their maturation into larger and shorter mushroom spines, but only dynamic studies can confirm this.

In CA1 pyramidal cells expressing TrkB.T1–EGFP or EGFP-F, no significant differences were seen in the densities of long ($P = 0.558$), thin ($P = 0.57$), or mushroom ($P = 0.065$) spines or filopodia ($P = 0.6$) (Fig. 3*B*). There was a moderate decrease of 35% in stubby spines ($P < 0.01$) in TrkB.T1–EGFP neurons. Together, these results show that postsynaptic TrkB signaling is an important regulator of adult spine morphology in adult V1 but much less so in CA1.

Reduced Mushroom Spine Maintenance of TrkB.T1–EGFP-Expressing Pyramidal Cells in V1 but Not in CA1. Over 70% of all spines in adult V1 are persistent for periods of months (7, 8). Our observation that 60% of mushroom spines disappear within 2 weeks of TrkB.T1–EGFP expression therefore suggests that spine maintenance is affected rather than the development of new mushroom spines. Because large mushroom spines are the most persistent (13), it is expected that spine loss due to natural turnover affects this population the least. However, the spine head diameter/length correlation plot (Fig. 4*A*) shows that mushroom spine heads of TrkB.T1–EGFP-expressing neurons are smaller than those of EGFP-F-expressing cells, with an almost complete loss of mushroom spines with head diameters >0.8 μm. Mushroom spines of TrkB.T1–EGFP-expressing neurons average a mean diameter of 0.49 μm compared with 0.78 μm of EGFP-F-expressing neurons ($P < 0.0001$, Fig. 4*B*). TrkB.T1–EGFP-expressing spines are also 30% longer than EGFP-F-expressing mushroom spines ($P < 0.0001$), with an average length of 1.5 μm. In CA1, mushroom spines of TrkB.T1–EGFP-expressing cells have an average head diameter of 0.7 μm and are similar to those of EGFP-F-expressing cells ($P = 0.69$, Fig. 4*D*). However, spine length increased by 32%, resulting in a mean length of 1.32 μm ($P < 0.0001$). This difference was mainly caused by increased spine length within the population of spines with heads <0.8 μm (38% increase, $P < 0.0001$ compared with 14% increase in larger spines, $P = 0.068$). Spine length distribution within this population was shifted upward, and spines longer than 1.5 μm increased from 2.5% in EGFP-F neurons to 35% in TrkB.T1–EGFP neurons ($P < 0.0001$, KS-Z value = 2.1) (Fig. 4*C*). Together, these data indicate that postsynaptic TrkB signaling in adult V1 pyramidal neurons is essential for the maintenance of mushroom spines although this finding does not seem to be true for CA1 neurons.

Decreased Miniature Excitatory Postsynaptic Current (mEPSC) Frequency and Amplitude in TrkB.T1–EGFP-Expressing Pyramidal Cells. Under normal circumstances, there is a good correlation between spine head size and synaptic efficacy. To test whether TrkB.T1–EGFP-induced reductions in mushroom spine density and head size had a functional correlate, we measured mEPSCs in neurons expressing EGFP-F ($n = 4$) and TrkB.T1–EGFP ($n = 4$). Amplitude and frequency of mEPSCs were markedly different in EGFP-F and TrkB.T1–EGFP-expressing neurons (Fig. 5). The average

distribution of time intervals between events was shifted toward larger intervals in TrkB.T1–EGFP-expressing neurons (Fig. 5*C*, $P < 0.0001$, KS-Z value = 11.28), resulting in a median interval of 0.62 ± 0.11 s and 0.19 ± 0.09 s in TrkB.T1–EGFP and EGFP-F-expressing cells, respectively. The average distribution of amplitudes was shifted toward smaller amplitudes in the TrkB.T1–EGFP-expressing cells (Fig. 5*D*, $P < 0.0001$, KS-Z = 7.44), resulting in a strong decrease in the number of events with amplitudes >25 pA. Median amplitudes of mEPSCs in TrkB.T1–EGFP and EGFP-F-expressing cells were 8.9 ± 0.03 pA and 10.95 ± 0.07 pA, respectively.

To exclude the possibility that the reduction of mEPSCs in TrkB.T1–EGFP-expressing cells was due to an acute effect of reduced TrkB signaling, mEPSCs were measured in slices of WT C57BL/6 mice in the absence or presence of a cell-permeable inhibitor of Trk phosphorylation, K252a ($n = 7$). The Friedman test showed that application of K252a in WT mice had no significant effect on either frequency ($P = 0.565$) or amplitude ($P = 0.779$) (data not shown).

Discussion

We examined the role of postsynaptic TrkB signaling in spine maintenance by expressing a dominant negative TrkB.T1–EGFP fusion protein in sparse pyramidal neurons of the adult neocortex and hippocampus of transgenic mice. This approach had several advantages over previously used models for studying the function of TrkB in cortical pyramidal cells. First, it permitted us to study morphological changes caused by interfering with TrkB-signaling in individual pyramidal neurons within an unaffected environment. Second, because synaptic partners of transgene-expressing neurons were genetically unaffected, pre- and postsynaptic influences of interfering with TrkB signaling could be discerned. Third, because expression of TrkB.T1–EGFP was confined to the adult brain (>6 wks), neuronal developmental was unaffected.

We found that, after 2 weeks of TrkB.T1–EGFP expression, spine morphology of pyramidal neurons in V1 had become reminiscent of neurons in the much younger visual cortex. Compared with EGFP-F-expressing neurons in adult V1, mushroom and stubby spines were reduced by 60–85% whereas the numbers of filopodia and long and thin spines had increased strongly. Even compared with pyramidal neurons in V1 of younger mice (5 wks), filopodia and thin spine types were more abundant and mature spine types were more reduced in TrkB.T1–EGFP-expressing neurons. These structural changes were accompanied by a reduction in both the amplitude and frequency of mEPSCs. The amplitude of mEPSCs is mainly a reflection of the number of AMPARs at the postsynaptic density, which in turn correlates with spine head size (12). Large mushroom spines show strong AMPA currents, whereas thinner spines may carry "silent synapses" containing *N*-methyl-D-asparate receptors but little or no AMPAR (11). In TrkB.T1–EGFP-expressing neurons, mEPSCs with large amplitudes disappeared almost entirely, and mEPSCs were smaller on the whole. This finding agreed well with the observed changes in mushroom head sizes (Fig. 4). The frequency of mEPSCs is influenced by the number of AMPAR-containing synapses and the efficiency of presynaptic vesicle release. In TrkB.T1–EGFP-expressing cells, the decrease in mEPSC frequency was twice that of the total spine density change but correlated with the reduction in mushroom and stubby spines. This result could imply that TrkB.T1–EGFP-expressing neurons had more silent synapses, which would fit the observed increase in immature-appearing spine types. However, we cannot rule out that presynaptic vesicle release was indirectly affected by postsynaptic changes caused by TrkB.T1–EGFP expression.

Previous experiments have shown that, during barrel cortex development, BDNF signaling through postsynaptic TrkB receptors is essential for the insertion of AMPARs at the postsynaptic density (40) and the development of mature synapses. As new spines also form and mature in adult V1, it is possible that this process is affected by postsynaptic expression of TrkB.T1–EGFP. What would the morphological consequences be of such a defect? Studies employing *in vivo* two-photon imaging have shown that, in adult V1, >70% of all spines are persistent (3, 7). Large mushroom spines are the most stable population (13). If the transition of long or thin spines into mushroom spines were to be inhibited for a 2-week time period in adult mice, we would expect to see a small reduction in the number of mushroom spines caused by natural turnover, with the population of large mushroom spines being least affected. In contrast, we found a strong decrease in the number of mushroom spines, with the largest mushroom spines disappearing altogether in TrkB.T1–EGFP-expressing neurons (Fig. 4*A*). Taken together, these findings indicate that reduced postsynaptic TrkB signaling results in reduced maintenance of large spines and a concomitant reduction in synaptic efficacy.

Recently, it was shown that TrkB deficiency in pyramidal neurons of adult CA1 had little effect on their total protrusion density (38). Because this finding contrasted with our observations in V1, we also analyzed spine morphologies of TrkB.T1–EGFP-expressing neurons in CA1. In agreement with the previous study, we observed no significant differences in spine densities of EGFP-F or TrkB.T1–EGFP-expressing pyramidal cells in CA1. Also, most spine subtypes were unaffected except for a 35% decrease in stubby spines (Fig. 3*B*). Head diameters of mushroom spines did not change, suggesting that postsynaptic TrkB is not involved in their maintenance. We did observe that small mushroom spines were longer, which may be an indication of reduced transition of long spines into mushroom spines due to TrkB.T1–EGFP expression (Fig. 4 *C* and *D*), but only dynamic imaging can confirm this. The different roles postsynaptic TrkB plays in the maintenance of spines in V1 and CA1 may well explain why long term TrkB deficiency results in the retraction of neurites and possibly degeneration of neurons in neocortex but not in hippocampus (41).

We observed that TrkB.T1–EGFP-expressing neurons in V1 had more long and thin spines and filopodia. The most intuitive explanation is that homeostatic mechanisms induced the formation of novel spines in an attempt to keep total synaptic input constant. A reduction in Ca^{2+} signaling due to the loss of synaptic input could lie at the basis of such a homeostatic response (19). In addition, some filopodia and thin and long spines may be retracting mushroom spines (8). Last, an increase in filopodia formation by truncated TrkB expression has also been observed in cultured hippocampal neurons. This effect was independent of BDNF, but involved p75 neurotrophin receptor (p75NTR) (42). We cannot exclude that the same process takes place in adult V1, in which case spine loss and the filopodia formation in TrkB.T1–EGFP-expressing neurons would be unrelated events. However, the low levels of p75NTR expression in cortical pyramidal cells and the lack of filopodia formation in the TrkB.T1–EGFP-expressing hippocampal neurons in which spine loss is much less prominent make this explanation less likely.

The results presented here define postsynaptic TrkB signals as an important determinant of synapse maintenance in V1. Therefore, the rise of BDNF levels in the developing visual cortex is likely to result in enhanced rigidity of its connections. The fact that TrkB.T1–EGFP-expressing neurons showed extensive changes in spine morphology in adult V1 indicates that the mature extracellular matrix does not inhibit structural plasticity altogether but supports the view that the extracellular matrix and TrkB signaling have synergistic roles in synaptic stability and maintenance (43).

Our observations also imply that, in V1, BDNF is capable of bidirectionally regulating synapse strength, with increased TrkB signaling resulting in synapse strengthening and decreased signaling resulting in synapse weakening. In this respect, it is remarkable that BDNF expression is reduced by stimuli associated with dendritic pruning, such as monocular deprivation (44), and that its release is reduced by stimuli inducing long-term depression (LTD) (45). Our

finding that signals through TrkB are directly or indirectly involved at maintaining AMPARs at the postsynaptic density may explain the observation that BDNF interferes with the induction of LTD in the visual cortex (33) and that monocular deprivation results in reduced surface expression of AMPARs (46).

It is striking that the same mechanism is not functional at the Schaffer collateral synapse where mushroom spine maintenance is not affected by postsynaptic TrkB.T1–EGFP expression. A possible mechanistic explanation for this difference is that AMPARs are expressed at much higher levels in hippocampus than in neocortex (47). This property may make hippocampal neurons less sensitive to TrkB-mediated differences in AMPAR expression (48) or trafficking (49) and, consequently, less prone to undergo structural changes. This difference seems compatible with the functions of synaptic plasticity in these areas. In V1, plasticity is mostly aimed at setting up and maintaining an efficient circuitry for the processing of visual input, which may be achieved effectively through structural changes that are less rapid and more permanent. Faster and less permanent forms of plasticity seem more appropriate for the temporary storage and transfer of information as occurs in hippocampus.

To comprehend the underlying biological mechanisms, it is imperative to determine whether TrkB signaling regulates synaptic stability at individual synapses or at the cellular level. It is also important to identify the site of BDNF release and to discern its autocrine and paracrine roles. Inactivation of the *bdnf* gene in isolated neurons and analyzing their spine and bouton morphology seems to be an appropriate approach for answering these questions.

Materials and Methods

DNA Constructs and Production of Transgenic Mice. Constructs for Cre-dependent expression of TrkB.T1–EGFP or EGFP-F were created as follows. The lox-Stop-lox (LSL) cassette from PBS302 (GIBCO/BRL, Bethesda, MD) was cloned into a Thy-1 promoter containing expression vector, rendering pThy-LSL. cDNA encoding amino acids 1–477 of TrkB and encompassing a 75-nt fragment of the 5′ untranslated region was cloned into the polylinker of EGFP-N3 (BD Biosciences). The fragment encoding TrkB.T1–EGFP was cloned into pThy-LSL rendering pThyLSL-TrkB.T1–EGFP. pThyLSL-EGFP-F was created by cloning the fragment encoding EGFP fused to the Ha-ras farnesylation site from pEGFP-F (BD Biosciences) into pThy-LSL. For production of transgenic mice expressing Cre under the control of the CaMKIIα promoter, pJTCre (50) was used (Fig. 6, which is published as supporting information on the PNAS web site).

Transgenic mice were created by pronuclear injections of linearized DNA into fertilized C57BL/6 oocytes. One of the seven ThyLSL-TrkB.T1–EGFP founders (TLT-817) showed sufficiently high EGFP levels for spine analysis. Nine ThyLSL-EGFP-F founders were obtained, of which three showed sufficient EGFP expression. Line TLG-498 was used in this study. Sparse labeling of pyramidal neurons in adult cortex was achieved by generating novel CaMKIIα-Cre transgenic mice. Four CaMKIIα-Cre founders were produced, of which two showed Cre recombination in a Golgi-staining-like pattern. Line Cre-3487 is described here. All experiments involving mice were approved by the institutional animal care and use committee of the Royal Netherlands Academy of Arts and Sciences.

Histology and Immunohistochemistry. Eight-week-old mice double transgenic for CaMKIIα-Cre and TrkB.T1–EGFP or EGFP-F were anaesthetized with 0.1 ml/g bodyweight Nembutal (Janssen) and perfused with 4% paraformaldehyde (PFA) in PBS and postfixed for 2 h. Coronal sections of 50 μm were made by using a vibratome (Leica VT1000S, Leica, Rijswijk, The Netherlands). To allow long-term storage and reduce bleaching, free-floating sections were stained by using mouse anti-GFP antibodies (1:500, Chemicon), followed by Alexa Fluor 568-conjugated goat anti-mouse antibodies (1:500, Invitrogen). Biocytin-injected slices (300 μm) were postfixed in 4% PFA and stained with chicken anti-GFP antibodies (1:1000, Chemicon), followed by Alexa Fluro 488-conjugated anti-chicken antibodies (1:500, Invitrogen) and Cy3-conjugated streptavidin (1:500, Vector Laboratories) for the detection of biocytin.

Diolistics. Diolistics were essentially performed as described (51). Briefly, 0.15 mg of DiI (Invitrogen) was mixed with 50 μl of methylene chloride and vortexed until completely dissolved. The dissolved dye was added to 12 mg of 1.1-μm tungsten particles (Bio-Rad) on a glass slide. This mixture was spread across the slide, and the solvent was allowed to evaporate for 2 min. The coated particles were transferred to a 1.5-ml tube, resuspended in 1 ml of distilled water, and sonicated. The suspension was sucked into Tefzel tubing (Bio-Rad) with a syringe, and the particles were allowed to settle for 2 min. The water was then withdrawn, and the tube was dried with a flow of nitrogen gas and cut into 13 mm pieces.

Fifty-micrometer coronal sections were shot by using the Helios Gene Gun (Bio-Rad) at 80 psi through a membrane filter with a 3-μm pore size and 8×10^5 pores/cm^2 (Corning). Sections were left for at least 12 h to ensure good filling of the labeled neurons.

Confocal Microscopy. EGFP-expressing, or DiI- or biocytin-labeled neurons from layer II/III of V1 or from CA1 were imaged by using a Carl Zeiss CLSM 510 Meta confocal microscope (Zeiss) with Argon (488 nm) and HeNe (543 nm) lasers. The first branch points of basal, proximal apical, and distal apical dendrites (Fig. 7*A*, which is published as supporting information on the PNAS web site) were imaged at a scaling of 60 nm ($\times$63 objective and an optical zoom of $\times$2.5) with 200-nm steps in the *z*-plane. The back-projected pinhole was 190 nm. For each image acquisition, the laser intensity and detector gain were adjusted so that the entire detector range was used for the spines. The image stacks were subjected to 3D reconstruction by using Zeiss CLSM 510 Meta. At these settings, spine morphology was not different from those that were subjected to blind deconvolution (Huygens Essential, Hilversum, The Netherlands).

Spine Classification and Image Analysis. Dendritic protrusions were classified as spines (mushroom, long, stubby, or thin) or filopodia and quantified as the number of protrusions per 15-μm segment (details in Fig. 7*B*). Spine analysis was performed on V1 neurons expressing EGFP-F (five mice, 19 neurons, 80 segments, and 1,447 spines) and TrkB.T1–EGFP (five mice, 25 neurons, 141 segments, and 1,970 spines) and on DiI-labeled neurons (2 mice, 10 neurons, 20 distal apical segments, 328 spines). For CA1 neurons, protrusions from basal and distal apical dendrites of neurons expressing EGFP-F (three mice, 11 neurons, 22 segments, and 454 spines) and TrkB.T1–EGFP (four mice, 8 neurons, 29 segments, and 535 spines) were quantified likewise.

Size determination of mushroom spines was carried out by using Zeiss CLSM IMAGE BROWSER 5 overlay tools. The longest straight line in the spine head was counted as the head diameter. The length of the entire spine (including head and stalk) was measured by using a bent-line tool. Spine size/length correlation plots were performed on mushroom spines from distal apical dendrites of neurons expressing EGFP-F (V1, 116 spines; CA1, 107) and TrkB.T1–EGFP (V1, 195 spines; CA1, 47). Statistical significance of differences in spine numbers per segment, spine length, or head size was determined by standard student's *t* test. Significance of differences in spine length distributions of CA1 mushroom spines was determined by the Kolmogorov-Smirnov (KS) test.

Electrophysiology. Coronal slices (300 μm) of V1 were prepared from 8- to 10-week-old mice. Animals were killed by decapitation, and brains were chilled in ice-cold carbogenated (95% O_2/5% CO_2) sucrose-based artificial cerebrospinal fluid (ACSF), containing 3.5 mM KCl, 2.4 mM $CaCl_2$, 1.3 mM $MgSO_4$, 1.2 mM KH_2PO_4, 10 mM glucose, 26 mM $NaHCO_3$, and 212.5 mM sucrose. Slices were stored in carbogenated normal ACSF comprising 126 mM NaCl, 3 mM KCl, 2 mM $MgSO_4$, 2 mM CaCl2, 10 mM Glucose, 1.20 mM NaH_2PO_4 and 26 mM NaHCO3 (305 mM mOsm and pH 7.3).

Slices were transferred to a submerged recording chamber with constant perfusion of carbogenated artificial cerebrospinal fluid. EGFP-expressing neurons in layer II/III of V1 were patched under an Axioskop FS upright microscope equipped with infrared differential interference contrast optics (Zeiss). Borosilicate glass patch-pipettes (4–6 MΩ) were filled with K-gluconate internal solution containing 154 mM K-gluconate, 1 mM KCl, 0.5 mM EGTA, 10 mM Hepes, 4 mM Mg-ATP, 4 mM K_2phosphocreatine, 0.4 mM GTP (pH 7.3 and 0.290 mosm), and 3 mg/ml biocytin (Invitrogen) for intracellular labeling. In whole-cell configuration, mEPSCs were recorded at 18–21°C by using a patch-clamp amplifier (EPC8, HEKA Electronics, Lambrecht, Germany) in the presence of 1 μM tetrodotoxin (Alomone Labs, Jerusalem) while holding the membrane potential at −70 mV.

K252a (Calbiochem, San Diego, CA) was applied to slices at 200 nM. After stabilization, mEPSCs were recorded for 9 min as baseline, 9 min in the presence of K252a, and 9 min after washing it out. Signals were low-pass filtered at 3.0 KHz and digitized at 10 KHz, with an ITC-16 computer interface (Instrutech, Mineola, NY). Care was taken that series resistance remained <20 MΩ.

Data Analysis. Mini Analysis (Synaptosoft Inc., Decatur, GA) was used for analyzing mEPSCs. The amplitude threshold was set at 7 pA, which was >3× root-mean-square (RMS) noise in all recordings. After automatic detection of mEPSCs by the software, each mEPSC was visually inspected. Recordings with a systematic drift in average mEPSC rise time of >10% were excluded. mEPSCs with rise times >3 ms were omitted. Frequencies and amplitude distributions of mEPSCs in EGFP-F versus TrkB.T1–EGFP neurons were compared for statistical significance by using the Kolmogorov-Smirnov test. Statistical analysis of the effect of K252a was done by using the Friedman test.

We thank Svetlana Skulj for technical assistance; Drs. Anthony Holtmaat, Andrew Matus, Martijn Roelandse, and Heinz Wässle for critical reading of the manuscript; Dr. Susumu Tonegawa for support in producing the CaMKIIα-Cre mice in his laboratory; Dr. Arjen Brussaard, Dr. Nail Burnashev, Johannes Lodder, and Jaap Timmerman for assistance with electrophysiology; and Dr. Chris Pool, Dr. Bob Nunes Cardozo, Koos de Vos, and Dr. Harry Uylings for advice on imaging and spine analysis. S.C. is supported by Rotterdamse Vereniging Blindenbelangen, Algemeen Nederlandse Vereeniging ter Voorkoming van Blindheid, and Stichting Blindenhulp. M.H.S. and M.B. are supported by the Netherlands Organization for Scientific Research (NWO). H.D.M. and C.N.L. are supported by the Royal Netherlands Academy of Arts and Sciences (KNAW) and NWO. C.N.L. is also supported by a ''Bsik'' grant from SenterNovem.

1. Hubel, D. H., Wiesel, T. N. & LeVay, S. (1977) *Philos. Trans. R. Soc. London B Biol. Sci.* **278,** 377–409.
2. Shatz, C. J. & Stryker, M. P. (1978) *J. Physiol.* **281,** 267–283.
3. Grutzendler, J., Kasthuri, N. & Gan, W. B. (2002) *Nature* **420,** 812–816.
4. Yuste, R. & Bonhoeffer, T. (2004) *Nat. Rev. Neurosci.* **5,** 24–34.
5. Fischer, M., Kaech, S., Knutti, D. & Matus, A. (1998) *Neuron* **20,** 847–854.
6. Wu, G. Y., Zou, D. J., Koothan, T. & Cline, H. T. (1995) *Neuron* **14,** 681–684.
7. Holtmaat, A. J., Trachtenberg, J. T., Wilbrecht, L., Shepherd, G. M., Zhang, X., Knott, G. W. & Svoboda, K. (2005) *Neuron* **45,** 279–291.
8. Zuo, Y., Lin, A., Chang, P. & Gan, W. B. (2005) *Neuron* **46,** 181–189.
9. Portera-Cailliau, C., Pan, D. T. & Yuste, R. (2003) *J. Neurosci.* **23,** 7129–7142.
10. Ziv, N. E. & Smith, S. J. (1996) *Neuron* **17,** 91–102.
11. Matsuzaki, M., Ellis-Davies, G. C., Nemoto, T., Miyashita, Y., Iino, M. & Kasai, H. (2001) *Nat. Neurosci.* **4,** 1086–1092.
12. Nusser, Z., Lujan, R., Laube, G., Roberts, J. D., Molnar, E. & Somogyi, P. (1998) *Neuron* **21,** 545–559.
13. Trachtenberg, J. T., Chen, B. E., Knott, G. W., Feng, G., Sanes, J. R., Welker, E. & Svoboda, K. (2002) *Nature* **420,** 788–794.
14. Matsuzaki, M., Honkura, N., Ellis-Davies, G. C. & Kasai, H. (2004) *Nature* **429,** 761–766.
15. Yuste, R. & Bonhoeffer, T. (2001) *Annu. Rev. Neurosci.* **24,** 1071–1089.
16. Nagerl, U. V., Eberhorn, N., Cambridge, S. B. & Bonhoeffer, T. (2004) *Neuron* **44,** 759–767.
17. Kirov, S. A. & Harris, K. M. (1999) *Nat. Neurosci.* **2,** 878–883.
18. Petrak, L. J., Harris, K. M. & Kirov, S. A. (2005) *J. Comp. Neurol.* **484,** 183–190.
19. Lohmann, C., Finski, A. & Bonhoeffer, T. (2005) *Nat. Neurosci.* **8,** 305–312.
20. Mataga, N., Mizuguchi, Y. & Hensch, T. K. (2004) *Neuron* **44,** 1031–1041.
21. Oray, S., Majewska, A. & Sur, M. (2004) *Neuron* **44,** 1021–1030.
22. Pizzorusso, T., Medini, P., Berardi, N., Chierzi, S., Fawcett, J. W. & Maffei, L. (2002) *Science* **298,** 1248–1251.
23. Galuske, R. A., Kim, D. S., Castren, E., Thoenen, H. & Singer, W. (1996) *Eur. J. Neurosci.* **8,** 1554–1559.
24. Cabelli, R. J., Hohn, A. & Shatz, C. J. (1995) *Science* **267,** 1662–1666.
25. Hanover, J. L., Huang, Z. J., Tonegawa, S. & Stryker, M. P. (1999) *J. Neurosci.* **19,** RC40.
26. Huang, Z. J., Kirkwood, A., Pizzorusso, T., Porciatti, V., Morales, B., Bear, M. F., Maffei, L. & Tonegawa, S. (1999) *Cell* **98,** 739–755.
27. Genoud, C., Knott, G. W., Sakata, K., Lu, B. & Welker, E. (2004) *J. Neurosci.* **24,** 2394–2400.
28. Gorski, J. A., Zeiler, S. R., Tamowski, S. & Jones, K. R. (2003) *J. Neurosci.* **23,** 6856–6865.
29. Horch, H. W., Kruttgen, A., Portbury, S. D. & Katz, L. C. (1999) *Neuron* **23,** 353–364.
30. Kovalchuk, Y., Hanse, E., Kafitz, K. W. & Konnerth, A. (2002) *Science* **295,** 1729–1734.
31. Castren, E., Pitkanen, M., Sirvio, J., Parsadanian, A., Lindholm, D., Thoenen, H. & Riekkinen, P. J. (1993) *NeuroReport* **4,** 895–898.
32. Korte, M., Carroll, P., Wolf, E., Brem, G., Thoenen, H. & Bonhoeffer, T. (1995) *Proc. Natl. Acad. Sci. USA* **92,** 8856–8860.
33. Akaneya, Y., Tsumoto, T. & Hatanaka, H. (1996) *J. Neurophysiol.* **76,** 4198–4201.
34. Kang, H. & Schuman, E. M. (1995) *Science* **267,** 1658–1662.
35. Murphy, D. D., Cole, N. B. & Segal, M. (1998) *Proc. Natl. Acad. Sci. USA* **95,** 11412–11417.
36. Shimada, A., Mason, C. A. & Morrison, M. E. (1998) *J. Neurosci.* **18,** 8559–8570.
37. Castren, E., Zafra, F., Thoenen, H. & Lindholm, D. (1992) *Proc. Natl. Acad. Sci. USA* **89,** 9444–9448.
38. Luikart, B. W., Nef, S., Virmani, T., Lush, M. E., Liu, Y., Kavalali, E. T. & Parada, L. F. (2005) *J. Neurosci.* **25,** 3774–3786.
39. Klein, R., Conway, D., Parada, L. F. & Barbacid, M. (1990) *Cell* **61,** 647–656.
40. Itami, C., Kimura, F., Kohno, T., Matsuoka, M., Ichikawa, M., Tsumoto, T. & Nakamura, S. (2003) *Proc. Natl. Acad. Sci. USA* **100,** 13069–13074.
41. Xu, B., Zang, K., Ruff, N. L., Zhang, Y. A., McConnell, S. K., Stryker, M. P. & Reichardt, L. F. (2000) *Neuron* **26,** 233–245.
42. Hartmann, M., Brigadski, T., Erdmann, K. S., Holtmann, B., Sendtner, M., Narz, F. & Lessmann, V. (2004) *J. Cell Sci.* **117,** 5803–5814.
43. Tropea, D., Caleo, M. & Maffei, L. (2003) *J. Neurosci.* **23,** 7034–7044.
44. Lein, E. S. & Shatz, C. J. (2000) *J. Neurosci.* **20,** 1470–1483.
45. Aicardi, G., Argilli, E., Cappello, S., Santi, S., Riccio, M., Thoenen, H. & Canossa, M. (2004) *Proc. Natl. Acad. Sci. USA* **101,** 15788–15792.
46. Heynen, A. J., Yoon, B. J., Liu, C. H., Chung, H. J., Huganir, R. L. & Bear, M. F. (2003) *Nat. Neurosci.* **6,** 854–862.
47. Petralia, R. S. & Wenthold, R. J. (1992) *J. Comp. Neurol.* **318,** 329–354.
48. Brene, S., Messer, C., Okado, H., Hartley, M., Heinemann, S. F. & Nestler, E. J. (2000) *Eur. J. Neurosci.* **12,** 1525–1533.
49. Jourdi, H., Iwakura, Y., Narisawa-Saito, M., Ibaraki, K., Xiong, H., Watanabe, M., Hayashi, Y., Takei, N. & Nawa, H. (2003) *Dev. Biol.* **263,** 216–230.
50. Tsien, J. Z., Chen, D. F., Gerber, D., Tom, C., Mercer, E. H., Anderson, D. J., Mayford, M., Kandel, E. R. & Tonegawa, S. (1996) *Cell* **87,** 1317–1326.
51. Benediktsson, A. M., Schachtele, S. J., Green, S. H. & Dailey, M. E. (2005) *J. Neurosci. Methods* **141,** 41–53.